arXiv:1608.07928v1 [physics.flu-dyn] 29 Aug 2016

Global stability analysis of axisymmetric boundary layers

Ramesh Bhoraniya Narayanan Vinod

September 19, 2016

Abstract

This paper presents the linear global stability analysis of the incompressible axisymmetric boundary layer on a circular cylinder. The base flow is parallel to the axis of the cylinder at inlet. The pressure gradient is zero in the streamwise direction. The base flow velocity profile is fully non-parallel and non-similar in nature. The boundary layer grows continuously in the spatial directions. Linearized Navier-Stokes(LNS) equations are derived for the disturbance flow quantities in the cylindrical polar coordinates. The LNS equations along with homogeneous boundary conditions forms a generalized eigenvalues problem. Since the base flow is axisymmetric, the disturbances are periodic in azimuthal direction. Chebyshev spectral collocation method and Arnoldi's iterative algorithm is used for the solution of the general eigenvalues problem. The global temporal modes are computed for the range of Reynolds numbers and different azimuthal wave numbers. The largest imaginary part of the computed eigenmodes are negative and hence the flow is temporally stable. The spatial structure of the eigenmodes shows that the flow is convectively unstable because the disturbance amplitudes grow in size and magnitude when moving towards downstream. The global modes of axisymmetric boundary layer are more stable than that of 2D flat plate boundary layer at low Reynolds number. However, at high Reynolds number they approaches to 2D flat plate boundary layer. Thus, the damping effect of transverse curvature is significant at low Reynolds number. The wave-like nature of the disturbances is found for most unstable eigenmodes.

1 Introduction

The linear stability analysis with the parallel base flow assumption is termed as local stability analysis where the base flow is varying only in wall normal direction. The linear stability of shear flows is governed by classical Orr-Sommerfeld equation. The numerical solutions to such problems deals with solutions of Orr-Sommerfeld equation obtained for disturbance amplitude functions are of wave-like nature. It is assumed that streamwise wavenumber is constant at each streamwise location and disturbance amplitude functions are a function of wall normal coordinate only. The numerical solution of Orr-Sommerfeld equation parallel base flow assumption can be achieved with very limited computational efforts [6]. The numerical solutions of Orr-Sommerfeld equation obtained for disturbance amplitude functions are of wave-like nature. It is assumed that

streamwise wavenumber is constant at each streamwise location and disturbance amplitude functions are a function of wall normal coordinate only. In spatially growing boundary layers, the base flow velocity is varying in streamwise direction which results in a considerable wall normal velocity. In these cases, non-parallel effects are very strong and cannot be neglected. This is true at low and moderate Reynolds numbers. The parallel flow assumption is not a good approximation for real flows where the flow is varying in streamwise direction. Under such conditions the flow becomes two-dimensional, and only wave-like nature of the solution is not expected. However, it may be one of the solution. Therefore, stability analysis with the parallel flow assumption may not represent the complete flow physics, and hence, it is having very limited scope for parallel and weakly non-parallel (WNP) flows only.

In the last decade, the stability analysis of non-parallel flow have received much attention through global stability analysis. Here the base flow is varying in both, radial and axial directions. The term global instability is used to represent instability analysis of the such flows [22]. The base flow considered here is non-parallel due to continuous growth of boundary layer in spatial directions and not self-similar due to transverse curvature effect [9, 26].
Global temporal modes are time harmonic solutions of the homogeneous linearized disturbance equations with homogeneous boundary conditions in space. Such solution obtained numerically for a base flow with strong non parallel effects [28]. If the base flow is varying slowly on the scale of a typical instability wavelength, global modes can be recovered by WKBJ type analysis [5]. A boundary layer at high Reynolds numbers and flow through diverging channels at small angles of divergence are common examples of weakly non-parallel flows. The boundary layer at low and moderate Reynolds number have strong non-parallel effects and hence WKBJ approach may not be the right choice. The prediction by non-parallel theory also agrees better with the experiments at moderate Reynolds numbers.
Joseph is the first among all to introduce the term global stability analysis, where he studied perturbation energy and established lower bounds for flow stability [11]. Bert reported the discovery of short-wavelength elliptic instability in inviscid vortex flows, a problem related to both transition and turbulence research. Bert discovered short-wavelength instability for inviscid vortex flow related to transition and turbulence research [2]. Jackson reports first computations on viscous flow where he studied flow past various shaped bodies [10]. onset of periodic behavior in two-dimensional laminar flow past bodies of various shapes is examined by means of finite-element simulations. Zebib studied growth of symmetric and asymmetric perturbations for flow past a circular cylinder [28]. They found that the symmetric disturbances are stable, the asymmetric perturbations become unstable at a Reynolds number about 40 with a Strouhal number about 0.12. The global approach is used by Christodoulou for free surface flow [3], Tatsumi for rectangular duct flow [20] and Lin for boundary layer flows [12]. The matrices generated by the discretization of global stability equations are very large, non-symmetric and sparse, which requires significant computational resources. All above said work have implemented QR algorithm for computations of eigenvalues and eigenvectors of resulting matrices. This algorithm computes all the eigenvalues. However, flow becomes unstable in case of a shear flow due to very few dangerous modes only, it is more economical

to calculate that modes only. Iterative techniques like Arnoldi's algorithm with shift-invert strategy computes few selected eigenvalues near the shift value. Theofilis studied 2D steady laminar separation bubble using WNP and DNS and got an excellent agreement of the stability results for both 2D and 3D [24]. By performing a global stability analysis, they proved the existence of new instability modes that are not explored by either of the approaches i.e. WNP & DNS. Theofilis studied the global stability of separated profiles in three different flow configurations, and they show that the amplitude of the global mode is less in the separated region than in the wake region or shear layer region [22] . Ehrenstein studied the global instability of a flat plate boundary layer [7] . By an optimal superposition of the global temporal modes, they were able to simulate the convective nature of instability of the boundary layer. Alizard performed a global stability analysis on a flat plate boundary layer and obtained an excellent agreement with the local stability results and the WNP results [1] . Monokrousos performed a global stability analysis of the flat plate boundary layer and calculated the maximum energy growth with a reduced order model and found that optimal energy growth can not be obtained with least stable global modes only but need to consider few globally stable modes also [15] . This is essential for flow control. Tezuka has first time solved initial value problem based on the same approach for three-dimensional disturbances [21] .

The study of stability analysis of incompressible axisymmetric boundary layer is found very sparse in literature. The available literature on axisymmetric boundary layers are limited to local stability analysis. Rao first studied the stability of axisymmetric boundary layer [16]. He found that non-axisymmetric disturbances are less stable than that of two-dimensional disturbances. The estimated critical Reynolds number based on free stream velocity and body radius of the cylinder was 11,000. Later work of Tutty investigated that for non-axisymmetric mode critical Reynolds number increases with azimuthal wave number N [25]. The critical Reynolds number found to be 1060 for N=1 mode and 12439 for N=0 mode. The axisymmetric mode is found least stable fourth mode. Recently Vinod investigated that higher non-axisymmetric mode $N = 2$ is linearly stable for a small range of curvature only [26] . The helical mode $N = 1$ is unstable over a significant length of the cylinder, but never unstable for curvature above 1. Thus, transverse curvature has overall stabilizing effect over mean flow and perturbations. Malik studied the effect of transverse curvature on the stability of incompressible boundary layer [14]. They investigated that the body curvature and streamline curvature are having significant damping effects on disturbances. They also found that traveling waves are the most amplified waves in three-dimensional boundary layers. The secondary instability of an incompressible axisymmetric boundary layer is also studied by Vinod [27]. They found that laminar flow is always stable at high transverse curvature to secondary disturbances. Parallel base flow assumption is considered in all above investigations.
The main aim of this paper is to study the global stability characteristics of the axisymmetric boundary layer and the effect of transverse curvature on it. The characteristics of the global eigenmodes of axisymmetric boundary layer are compared with the flat plate boundary layer(with zero transverse curvature) at different Reynolds numbers.The comparison shows that the transverse curvature has overall stabilizing effect on the disturbances.

2 Problem formulation

We follow the standard procedure to derive Linearized Navier-Stokes equations for disturbance flow quantities. The Navier-Stokes equations for mean flow and instantaneous flow are written in polar cylindrical coordinates (r, θ, x). The equations are non-dimensionalised using free stream velocity (U_∞) and displacement thickness (δ^*) at the inlet of the domain. Following the standard procedure of stability analysis, we get the set of equations for disturbance flow quantities. The base flow is axisymmetric and disturbances are three-dimensional in nature. The Reynolds number is defined as,

$$R_e = \frac{U_\infty \delta^*}{\nu} \tag{1}$$

The flow quantities are split into base flow and perturbations,

$$\overline{U} = U + u, \overline{V} = V + v, \overline{W} = 0 + w, \overline{P} = P + p, \tag{2}$$

We assume normal mode form for disturbances with amplitude varying in radial(r) and streamwise(x) directions. It is correct to assume periodicity in azimuthal(θ) direction as the flow is axisymmetric.

$$q(x, r, t) = \hat{q}(x, r) e^{[i(N\theta - \omega t)]} \tag{3}$$

where,
q = [u, v, w, p]
Q = [U, V, W, P]
$\overline{Q} = [\overline{U}, \overline{V}, \overline{W}, \overline{P}]$
ω = frequency of the waves
N= azimuthal wave number
U_∞=free stream velocity
δ^* = displacement thickness
a = body radius of the cylinder

where, q , Q and $\overline{Q}$ are the perturbation, mean and instantaneous flow quantities respectively. u ,v and w are the disturbance velocity components in the axial(x), radial(r) and azimuthal(θ) directions respectively. The Linearized Navier-Stokes equations for instability analysis are as follows,

$$\frac{\partial u}{\partial t} + U\frac{\partial u}{\partial x} + u\frac{\partial U}{\partial x} + V\frac{\partial u}{\partial r} + v\frac{\partial U}{\partial r} + \frac{\partial p}{\partial x} - \frac{1}{Re}[\bigtriangledown^2 u] = 0 \tag{4}$$

$$\frac{\partial v}{\partial t} + U\frac{\partial v}{\partial x} + u\frac{\partial V}{\partial x} + V\frac{\partial v}{\partial r} + v\frac{\partial V}{\partial r} + \frac{\partial p}{\partial r} - \frac{1}{Re}[\bigtriangledown^2 v - \frac{v}{r^2} - \frac{2}{r^2}\frac{\partial w}{\partial \theta}] = 0 \tag{5}$$

$$\frac{\partial w}{\partial t} + U\frac{\partial w}{\partial x} + V\frac{\partial w}{\partial r} + V\frac{w}{r} + \frac{1}{r}\frac{\partial p}{\partial \theta} - \frac{1}{Re}[\bigtriangledown^2 w - \frac{w}{r^2} + \frac{2}{r^2}\frac{\partial v}{\partial \theta}] = 0 \tag{6}$$

$$\frac{\partial u}{\partial x} + \frac{\partial v}{\partial r} + \frac{v}{r} + \frac{1}{r}\frac{\partial w}{\partial \theta} = 0 \tag{7}$$

where,

$$\bigtriangledown^2 = \frac{\partial^2}{\partial x^2} + \frac{\partial^2}{\partial r^2} + \frac{1}{r}\frac{\partial}{\partial r} + \frac{1}{r^2}\frac{\partial^2}{\partial \theta^2} = 0 \tag{8}$$

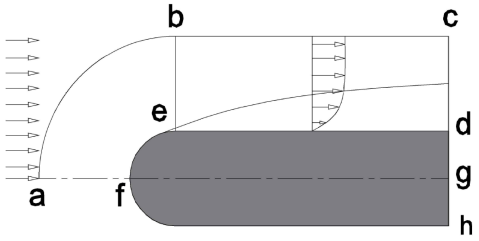

Figure 1: Schematic diagram of axisymetirc boundary layer on a circular cylinder. Dotted line represents the domain for stability computations.

2.1 Boundary conditions

At wall, on the solid surface of cylinder no slip and no penetration boundary conditions are applied. All disturbance velocity components have zero magnitude at the solid surface of the cylinder.

$$u(x,a) = 0,\ v(x,a) = 0,\ w(x,a) = 0 \tag{9}$$

At free stream far away from the surface of cylinder exponential decay of disturbances is expected. Homogeneous Dirichlet boundary conditions are applied for velocity and pressure disturbances at free-stream.

$$u(x,\infty) = 0,\ v(x,\infty) = 0,\ w(x,\infty) = 0,\ p(x,\infty) = 0 \tag{10}$$

The boundary conditions in streamwise direction are not straight forward. Homogeneous Dirichlet boundary conditions are applied on disturbance velocity components at the inlet. This boundary condition is appropriate as suggested by Theofilis (2003) because we are interested in the disturbances evolved within the basic flow field only. At outlet one may apply boundary conditions based on the incoming/outgoing wave information [8]. Such conditions impose wave-like nature of the disturbances and it is more restrictive in nature. This is not appropriate from the physical point of view in instability analysis. Even the wave number α is not known initially in case of a global stability analysis. An alternative way is to impose numerical boundary condition which extrapolate information from the interior of the computational domain. Linear extrapolated conditions are applied by several investigators. Review of literature on global stability analysis suggests linearly extrapolated boundary conditions are the good approximations [22, 19]. We also tried second order extrapolated boundary conditions, however the difference is only marginal. Thus, we considered linear extrapolated conditions at outlet.

$$u(x_{in},r) = 0,\ v(x_{in},r) = 0,\ w(x_{in},r) = 0, \tag{11}$$

$$u_{n-2}[x_n - x_{n-1}] - u_{n-1}[x_n - x_{n-2}] + u_n[x_{n-1} - x_{n-2}] = 0 \tag{12}$$

Similarly, one can write extrapolated boundary conditions for wall normal and azimuthal disturbance components v and w respectively. The boundary conditions for pressure do not exist physically at the wall. However, compatibility

conditions derived from the Linearized Navier-Stokes equations are collocated at the wall of cylinder [22] .

$$\frac{\partial p}{\partial x} = \frac{1}{Re}[\bigtriangledown^2 u] - U\frac{\partial u}{\partial x} - V\frac{\partial u}{\partial r} \tag{13}$$

$$\frac{\partial p}{\partial r} = \frac{1}{Re}[\bigtriangledown^2 v] - U\frac{\partial v}{\partial x} - V\frac{\partial v}{\partial r} \tag{14}$$

The Linearized Navier-Stokes equations are discretized using Chebyshev spectral collocation method. The Chebyshev polynomial generates non-uniform grids and generates more collocation points towards the ends. It is a favourable arrangement for the boundary value problems.

$$x_{cheb} = \cos(\frac{\pi i}{n}) \quad \text{where} \quad i = 0, 1, 2, 3....n \tag{15}$$

$$y_{cheb} = \cos(\frac{\pi j}{m}) \quad \text{where} \quad j = 0, 1, 2, 3....m \tag{16}$$

Where n and m are number of collocation points in streamwise and wall normal direction. The gradient of disturbance amplitude functions is very large near the wall region within the thin boundary layer, which requires a large number of grid points to increase the spatial resolution. Grid stretching is applied via the following algebraic equation [13].

$$y_{real} = \frac{y_i * L_y * (1 - y_{cheb})}{L_y + y_{cheb} * (L_y - 2y_i)} \tag{17}$$

In the above grid stretching method, half number of the collocation points are concentrated within the y_i distance from the lower boundary only. The non-uniform nature of distribution for collocation points in the streamwise direction is undesirable. The maximum and minimum distance between the grid points are at center and end respectively. Thus, it makes a poor resolution at the center of the domain and a very small distance between the grids at the end gives rise to Gibbs phenomenon. To improve the resolution and to minimize the Gibbs oscillation in the solution, grid mapping is implemented in streamwise direction using following algebraic equation [4] .

$$x_{map} = \frac{sin^{-1}(\alpha_m x_{cheb})}{sin^{-1}(\alpha_m)} \tag{18}$$

The value of α_m is selected carefully to improve spatial resolution in the streamwise direction. A very small value of α_m keeps the grid distribution like Chebyshev and near to unity almost uniform grid. For the detail description of the grid mapping readers are suggested to refer [4]. To incorporate the effect of physical dimensions of the domain [L_x, L_y] along with grid stretching and mapping it is required to multiply the Chebyshev differentiation matrices by proper Jacobean matrix. Once all the partial derivatives of the LNS are discretized by spectral collocation method using Chebyshev polynomials, the operator of the differential equations formulates the matrices A and B. These matrices are square, real and sparse in nature, formulates general eigenvalues problem.

$$\begin{bmatrix} A_{11} & A_{12} & A_{13} & A_{14} \\ A_{21} & A_{22} & A_{23} & A_{24} \\ A_{31} & A_{32} & A_{33} & A_{34} \\ A_{41} & A_{42} & A_{43} & A_{44} \end{bmatrix} \begin{bmatrix} u \\ v \\ w \\ p \end{bmatrix} = i\omega \begin{bmatrix} B_{11} & B_{12} & B_{13} & B_{14} \\ B_{21} & B_{22} & B_{23} & B_{24} \\ B_{31} & B_{32} & B_{33} & B_{34} \\ B_{41} & B_{42} & B_{43} & B_{44} \end{bmatrix} \begin{bmatrix} u \\ v \\ w \\ p \end{bmatrix} \tag{19}$$

$$[A][\phi] = i\omega[B][\phi]$$

where A and B are square matrix of size 4nm, $i\omega$ is an eigenvalues and ϕ is a vector of unknown amplitude of disturbance flow quantities u, v, w and p. The above mentioned all the boundary conditions are properly incorporated in the matrix A and B.

2.2 Solution of general eigenvalues problem

The matrix A and B are sparse in nature and of very large size. For $n = 121$ and $m = 121$ the number of eigenvalues are 58564. i.e. in the order of $(10^4 to 10^5)$. The eigenvalues problem being very large to solve for all the eigenvalues. However for instability analysis, the few eigenvalues with its largest imaginary parts, which makes the flow temporally unstable, are important. Hence, we are interested in the few eigenvalues and corresponding eigenvectors only. The QZ algorithm computes the full spectrum of eigenvalues and hence obviously it is not economical. The iterative method based on Arnoldis algorithm is a proper choice. The Krylov subspace provides the possibility of extracting major part of the spectrum using shift and invert strategy. The computations of Krylov subspace along with Arnoldi's algorithm applied to eigenvalues problem becomes easy.

$$(A - \lambda B)^{-1} B\phi = \mu\phi \quad where \quad \mu = \frac{1}{i\omega - \lambda} \tag{20}$$

Where, λ being the shift parameter and μ is the eigenvalues of the converted problem. Sometimes it is also called spectral transformation, which converts generalized eigenvalues problem to standard eigenvalues problem. The Krylov subspace may be computed by successive resolution of the linear system with matrix $(A - \lambda B)$, using LU decomposition. Full spectrum method is employed for this small subspace to get a good approximate solution to the original general eigenvalues problem [23]. The large size of the Krylov subspace extracts major part of the spectrum. Generally, the computed spectrum is always nearby the shift parameter. The good approximation of shift parameter reduces the number of iterations to converge the solution to required accuracy level. However, larger size of subspace makes the solution almost independent from the shift parameter λ. We tested the code for several values of shift parameter λ. The convergence of the solution depends on the value of shift parameter. The good approximation of the shift value needs less number of iterations. However we have taken the maximum number of iterations equal to 300; hence convergence of the solution may not be affected by shift parameter. Given the large subspace size of $k = 250$, the part of the spectrum for our instability analysis could be recovered in the one computation that took about 2.36 hours on Intel Xenon(R) CPU E5 26500@2.00$GHz \times 18$.

3 Base flow solution

The base flow velocity profile is obtained by solving the steady Navier-Stokes equations (21)-(23)with the finite-volume code ANSYS Fluent. The axisymmetric domain is considered with 20 and 200 radius in radial and axial directions

as shown in figure 1.

$$U\frac{\partial U}{\partial x}+V\frac{\partial U}{\partial r}=-\frac{\partial P}{\partial x}+\frac{1}{R_e}(\frac{\partial^2 U}{\partial x^2}+\frac{1}{r}\frac{\partial U}{\partial r}+\frac{\partial^2 U}{\partial r^2}) \tag{21}$$

$$U\frac{\partial V}{\partial x}+V\frac{\partial V}{\partial r}=-\frac{\partial P}{\partial r}+\frac{1}{R_e}(\frac{\partial^2 V}{\partial x^2}+\frac{1}{r}\frac{\partial V}{\partial r}+\frac{\partial^2 V}{\partial r^2}) \tag{22}$$

$$\frac{\partial U}{\partial x}+\frac{\partial V}{\partial r}+\frac{V}{r}=0 \tag{23}$$

Appropriate boundary conditions are applied to close the formulation of above problem. Uniform streamwise velocity U_∞ was imposed at the inlet (ab) and no-slip and no penetration boundary conditions at the surface of the cylinder (fed). Slip boundary condition($\mathbf{n}.\mathbf{U}=0$) was imposed at free stream far away from the solid surface (bc) and outflow boundary conditions at outlet(cd), that consists $\frac{\partial U}{\partial x}=0$, $\frac{\partial V}{\partial x}=0$ and $P=0$. Line afg is the axis of the cylinder. The steady Navier-Stokes equations was solved using SIMPLE algorithm with under-relaxation , to get a stable solution . Quick, a weighted average of second order upwind and second order central scheme was used for spatial discretization of momentum equations. Thus obtained base flow velocity profile is interpolated to spectral grids using cubic spline interpolation to perform global stability analysis. The solution for the base flow has converged with the total 251251 number of grid points with 1001 and 251 grids in streamwise and radial directions respectively. The distribution of the grids is geometric in both the directions. We started simulation initially with coarse grid size of 501 and 125 grids in axial and radial direction and refined it with a factor of 1.4142 in each directions. The discretization error was computed through Grid Convergence Index study on three consecutive refined grids[17]. The monotonic convergence is found for all this refined grids. In our problem we computed error and GCI for two field values U(x=75,r=1.2) and V(x=75,r=1.2) near the surface of the cylinder, where the gradient of the velocity field is maximum. The GCI and error was computed for three different grids as shown table 1 The error between Mesh 1 and Mesh 2 is too small. The GCI has also reduced with the increased spatial resolution. It shows that solution is converging monotonically towards the grid-independent one. Further refinement in the grid will hardly improve the accuracy of the solution while increases the time for the computations. The grid is thoroughly refined near the wall where velocity gradient is very high. The convergence order n for U and V is 2.00, which is in agreement with the second order discretization scheme used in the finite volume code ANSYS FLUENT. A Mesh 1 was checked with domain height of 25 times cylinder radius to study the effect of far-field condition. The percentage error with this two domain height is within 0.1 %. Thus, Mesh 1 was used in all the results presented here in to compute velocity field for the base flow.

4 Code validation

For the purpose of preliminary comparisons of global stability results with local stability results, we reduced the global nature of the problem to an equivalent local stability problem. The domain length equal to one wavelength (Lx=$2\pi/\alpha$) is taken in streamwise direction for a least stable axisymmetric mode(N=0).

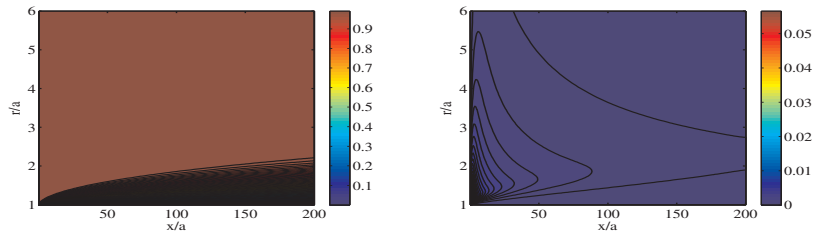

Figure 2: Base flow velocity profile for streamwise (U) and normal(V) velocity components for $R_e = 2000$. The Reynolds number is calculated based on body radius of the cylinder. The velocity profile is interpolated to collocation points for instability analysis. The actual domain height in wall normal direction is 20 radius of the cylinder.

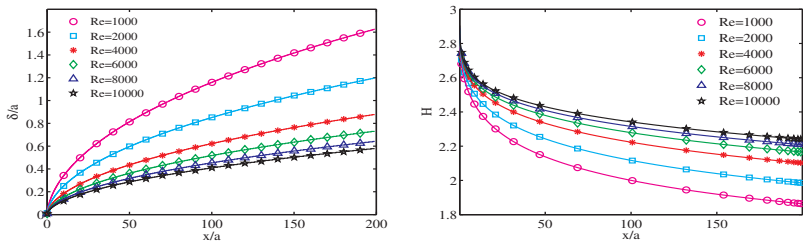

Figure 3: Variation of transverse curvature (δ/a)(left) and shape factor(H)(right) in streamwise direction for different Reynolds number. Reynolds number is based on body radius(a) of the cylinder. Axial and radial length is normalized with cylinder radius (a).

Table 1: The Grid Convergence study for the base flow is obtained , using U(x=75,r=1.2) and V(x=75,r=1.2) for Re=1000. The grid refinement ratio(α)in each direction is 1.4142. The relative error(ϵ) and Grid Convergence Index (GCI) are calculated using two consecutive grid size. The j and j+1 represents course and fine grids respectively. ϵ=$\frac{f_j - f_{j+1}}{f_j}$ $\times$ 100. $GCI(\%)$=3[$\frac{f_j - f_{j+1}}{f_{j+1}(\alpha^n - 1)}$] $\times$ 100, where n=log[$\frac{f_j - f_{J+1}}{f_{j+1} - f_{j+2}}$]/log($\alpha$) .

Mesh	Grid size	U	ϵ(%)	GCI(%)	V	ϵ(%)	GCI(%)
#1	1001 $\times$ 251	0.034138	0.00879	0.0262	1.655$\times$ 10^{-5}	0.060	0.1812
#2	708 $\times$ 177	0.034135	0.0175	0.05274	1.656$\times$ 10^{-5}	0.12	0.3622
#3	501 $\times$ 125	0.034129	–	–	1.658$\times$ 10^{-5}	–	–

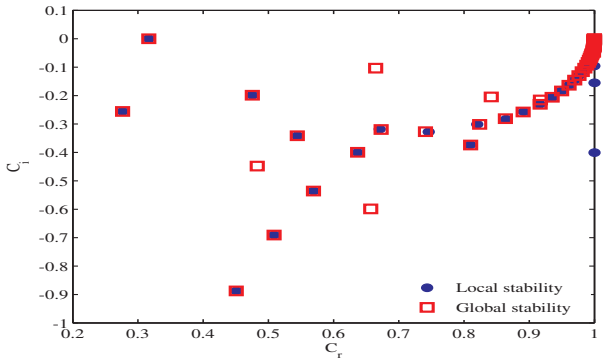

Figure 4: Comparison of eigenspectrum for local and global stability analysis for axisymmetric mode (N=0) and Reynolds number $R_e = 12439$. Here $R_e = 12439$ is a critical Reynolds number for local stability analysis based on body radius of the cylinder.

Non-parallel effects from the mean flow velocity profile are removed to apply parallel flow assumption i. e. $V = 0$ & $\frac{\partial U}{\partial x} = 0$. In wall normal direction, the boundary conditions are same as that of local stability analysis [22]. To impose wave-like behaviour of disturbances, Robin and periodic boundary conditions are applied in the streamwise direction at inlet and outlet [19] . The Robin boundary conditions with constant streamwise wavenumber α is prescribed at inlet and outlet. The Robin boundary conditions are derived from the $\phi(r,t) = \hat{\phi}(r)e^{[(i(N\theta-\omega t)]}$. We applied Robin boundary conditions along with periodic boundary conditions at inlet and outlet with constant streamwise wavenumber α.

$$\frac{\partial^2 u}{\partial x^2} = -\alpha^2 u, \frac{\partial^2 v}{\partial x^2} = -\alpha^2 v \tag{24}$$

$$u(x,r) = u(x+Lx,r), v(x,r) = v(x+Lx,r) \tag{25}$$

Above boundary conditions are applied to disturbance velocity components in a streamwise direction at inlet and outlet. The second derivatives are considered to avoid complex quantities in the boundary conditions and hence fast computations can take place. Here we considered axisymmetric mode($N = 0$) for the validation of global stability results. The critical Reynolds number, streamwise wavenumber and streamwise location are 12439, 2.73 and 47 respectively [25]. The Reynold number is based on the body radius of the cylinder. Streamwise domain length is taken equal to one wavelength($L_x = 2.3015$). The domain in streamwise direction is very limited and hence the solution is converged with the number of collocation points n=41 in streamwise direction and m=101 in the radial direction. The eigenspectrum and eigenfunctions are in good agreement with the results of local stability analysis as shown in figure 4 and figure 5. The streamwise wavenumber α is computed from the eigenfunctions obtained through global stability analysis and it is equal to 2.73. Hence, the applied value of α is recovered in the global stability analysis. The perturbation for the disturbances u and v can be written as $u = ue^{[i\theta_u(x,r)]}$ and , $v = ve^{[i\theta_v(x,r)]}$, where θ_u and θ_v are phase angles of wave with respect to x and

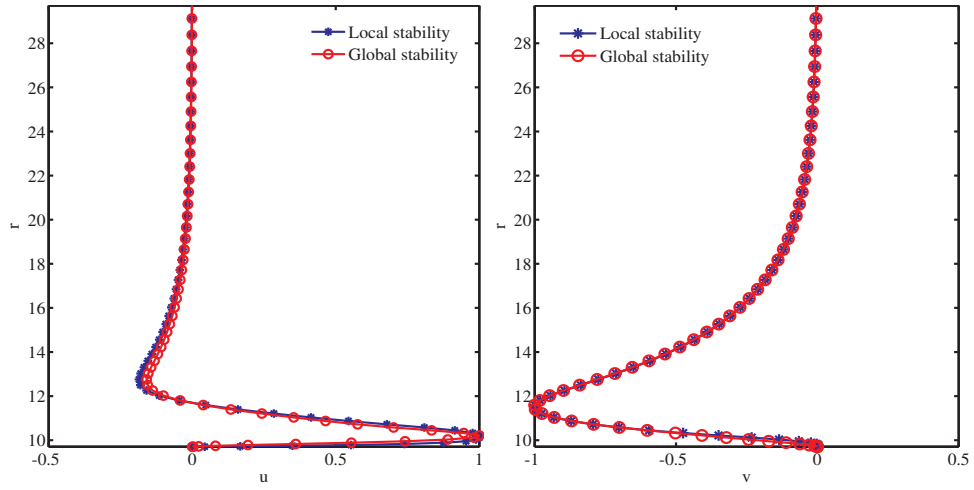

Figure 5: Comparisons of the real parts of (a) streamwise u and (b) wall normal v eigen functions for local and global stability analysis for axisymmetric mode (N=0) for Reynolds number $R_e = 12439$ based on body radius of the cylinder. The Reynolds number based on the displacement thickness (δ^*) is 1264.

r. The phase angles of waves can be defined by the following relationship [1].

$$\theta_u = tan^{-1}(\frac{u_i}{u_r}), \theta_v = tan^{-1}(\frac{v_i}{v_r}) \tag{26}$$

Where r and i denotes real and imaginary parts of the eigenfunctions u and v. The phase is dependent on the normal coordinate only. Thus the position of maximum absolute magnitude of each disturbances remains same at all the streamwise locations. The streamwise wave number (α) is calculated by [1].

$$\alpha_{ru} = \frac{\partial \theta_u(x, y_{umax})}{\partial x}, \alpha_{rv} = \frac{\partial \theta_v(x, y_{vmax})}{\partial x} \tag{27}$$

5 Results and discussions

In the present analysis Reynolds number is varying from 261 to 693 with azimuthal wave numbers 0, 1, 2, 3, 4 and 5. Reynolds number based on the displacement thickness (δ^*) at the inlet of the domain is considered. Streamwise and wall normal dimensions are normalized with the displacement thickness at the inlet of the domain. The streamwise domain length $L_x = 345$ and wall normal height $L_r = 20$ is selected for the instability analysis. The number of collocation points considered are $n = 121$ in streamwise direction and m=121 in wall normal direction. The general eigenvalues problem is solved using ARPACK, which uses Arnoldi's algorithm. The computed eigenvalues are found to be accurate up to three decimal points. The additional lower resolution cases were also run to confirm the proper convergence of the eigenspectrum. Heavy sponging is applied to avoid the spurious reflections at the outlet. The eigenvalues with the largest imaginary part that is least stable ones is selected. The two-dimensional mode structure of the selected modes is also checked for

Table 2: The Grid Convergence study for two leading eigenvalues ω_1 and ω_2 for $R_e = 383$ and N=1 for different grid size. The grid refinement ratio in each direction is 1.14. The maximum relative error is shown here .

Mesh	Lx	Lr	n×m	n	m	ω_1	ω_2	error(%)
#1	605	20	14641	121	121	0.03654-0.01763i	0.02965-0.01770i	3.1598
#2	605	20	11449	107	107	0.03644-0.01709i	0.02951-0.01751i	6.3791
#3	605	20	8649	93	93	0.03636-0.01642i	0.02938-0.01646i	—

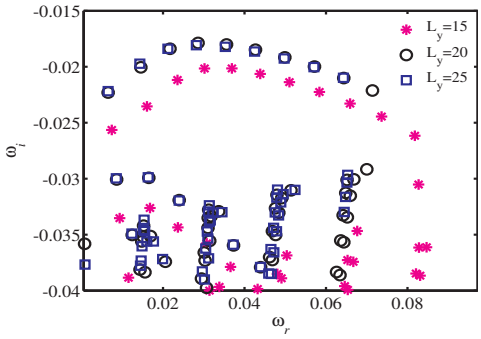

Figure 6: Eigenspectrum for azimuthal wavenumber N=1 and Re=383 for three different domain height Lr=15, 20 and 25.

the spurious mode.

5.1 Grid convergence study

A grid convergence study was performed to check the accuracy of the solution and appropriate grid size. Table 2 shows the values of two leading eigenvalues computed for $Re = 383$ for axisymmetric mode using different three grid size. The grid resolution was successively improved by a factor of 1.14 in axial and radial direction respectively. The real and imaginary parts of the eigenvalues shows monotonic convergence of the solution with the increase in resolution. In this table n and m indicates the number of grids in axial and radial directions respectively. The relative errors are calculated between consecutive grids for real and imaginary parts of the eigenvalues. The largest associated error among both the eigenmode is considered. The relative error for mesh 1 is well within the limit and it is used for all the results reported here. To check the influence of domain height(Lr), computations were performed with three different domain height of Lr=15,20 and 25. The difference of results obtained with Lr=20 and Lr=25 is too small as shown in figure 6. Thus Lr=20 is selected for all global stability computations.

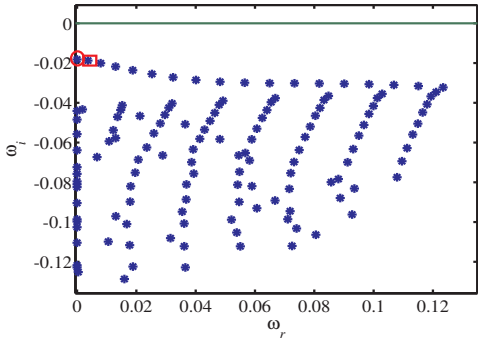

Figure 7: Eigenspectrum for azimuthal wavenumber N=0 (axisymmetric mode) and Re=383.

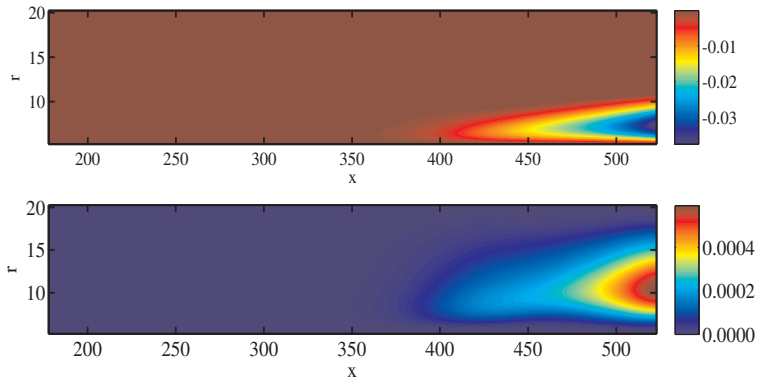

Figure 8: Contour plot of stationary mode (a) streamwise velocity and (b) normal velocity for the eigenvalue $\omega = 0.0 - 0.01818i$, as marked by circle in figure 7 .

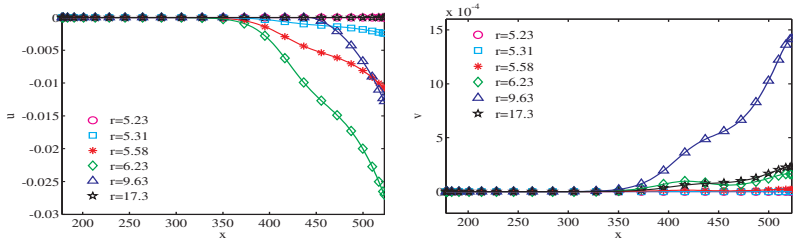

Figure 9: Variation of disturbance amplitudes in streamwise direction for stationary mode (a) streamwise velocity (u) and (b) normal velocity(v) for the eigenvalue $\omega = 0.0 - 0.01818i$, as marked by circle in figure 7 .

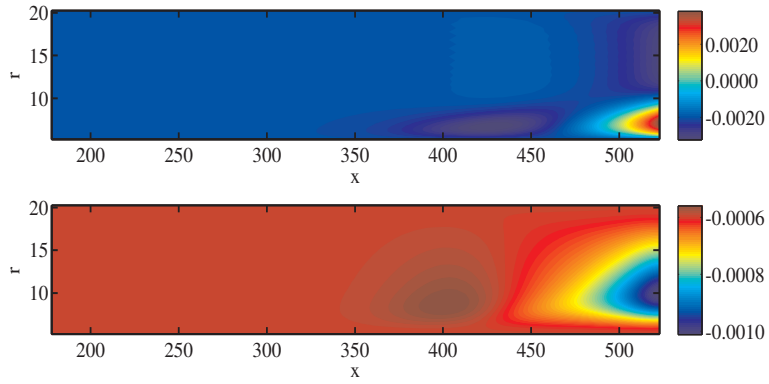

Figure 10: Contour plot of oscillatory mode (a) streamwise velocity and (b) normal velocity for the eigenvalue $\omega = 0.003689 - 0.01874i$, as marked by square in figure 7 .

5.2 Axisymmetric mode

Figure 7 shows the eigenspectrum for the axisymmetric mode (N=0) with Reynolds number, $Re = 383$. In figure 7, the eigenmodes marked by circle and square are stationary ($\omega_r = 0$) and oscillatory($\omega_r > 0$) modes respectively. The stationary mode has a complex frequency $\omega = 0 - 0.01818i$. This global mode is temporally stable because $\omega_i < 0$ and hence disturbances decay in time. Figure 8 shows the two dimensional spatial structure of the streamwise(u) and wall normal (v) disturbance amplitudes for stationary mode $\omega = 0 - 0.01818i$. The magnitudes of the velocity disturbances is zero at the inlet, as it is the inlet boundary condition. As the fluid particles move towards the downstream, the disturbances evolve monotonically in time within the domain and progresses towards the downstream. The magnitude of the u disturbance amplitudes is one order higher than that of v disturbance amplitudes. The amplitude structure has opposite sign for u and v. The spatial structure of the amplitudes grow in size and magnitude towards the downstream. Figure 9 shows the variation of u and v disturbance amplitudes in streamwise direction at different radial locations. The magnitude of the disturbance amplitudes are very small near the cylinder surface due to viscous effect, increases in radial direction and vanishes at far-field.

The most unstable oscillatory mode has an eigenvalue $\omega = 0.003689 - 0.01874i$. The flow is stable for this global mode because $\omega_i < 0$. The spatial structure of the above global eigenmode for u and v disturbance amplitudes are not monotonic in nature.The distribution in spatial directions is show in figure 10 . The amplitudes of the velocity disturbances is zero at the inlet as it is the imposed boundary condition at the inlet . However, in the streamwise direction the disturbances grow in magnitudes and it contaminates the flow field towards the downstream. The magnitudes of the disturbance amplitudes grows exponentially as they move further towards the downstream and hence flow is convectively unstable [18]. However, its variation in the normal direction is different from that of a stationary mode, as seen in the respective figures. The magnitude of the normal disturbance amplitudes is one order less than that of the

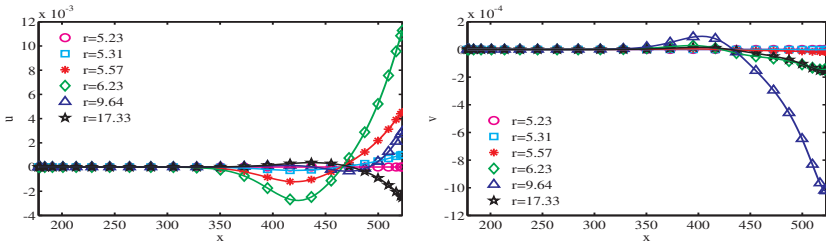

Figure 11: Variation of disturbance amplitudes in streamwise direction for oscillatory mode (a)streamwise velocity (u) and (b) normal velocity(v) for the eigenvalue $\omega = 0.003689 - 0.01874i$, as marked by square in figure 7 .

streamwise component.
Figure 11 presents variation of disturbance amplitudes in streamwise direction at various radial locations. It shows that the most of the disturbances grow in magnitude as they move towards downstream. The magnitude of the disturbance amplitudes are very small near the wall due to viscous effect, gradually increases in radial direction and finally vanishes at the far-field. It shows that disturbances evolve within the flow-field in time and grow in magnitude and size while moving towards the downstream.

5.3 Effect of frequency on eigen function

Figure 12 shows contour plot of the real part of streamwise disturbance velocity of two different eigen modes with frequency ω_r=0.003689 & ω_r=0.1234 for N=0 and Re=383. The streamwise domain length is 345. The disturbances is seen to evolve in the vicinity of the wall and increasing the amplitudes when moving towards downstream. The typical length scale of the the wavelet structure decreases with the increases in frequency(ω_r) .

5.4 Effect of transverse curvature

The body radius of the cylinder is another important length scale in case of the axisymmetric boundary layer in addition to the boundary layer thickness (δ^*). The inverse of the body radius is called the transverse surface curvature(S). The flat plate boundary layer is a special case of a zero transverse curvature. It is normalised with the displacement thickness (δ^*) at the inlet. In case of the axisymmetric boundary layer it has significant effect on the characteristic of base flow as well as disturbance flow quantities. In order to understand the transverse curvature effect on the stability characteristic of the axisymmetric boundary layer,the stability characteristics are compared with the flat plate boundary layer(zero transverse curvature) at the same Reynolds number and domain size. The Reynolds number is computed based on the displacement thickness and free-stream velocity at the inlet. The eigen spectrum, spatial amplification rate, effect of the domain length on the distribution of the spectrum and eigen functions are compared at the same Reynolds number. Figure 13

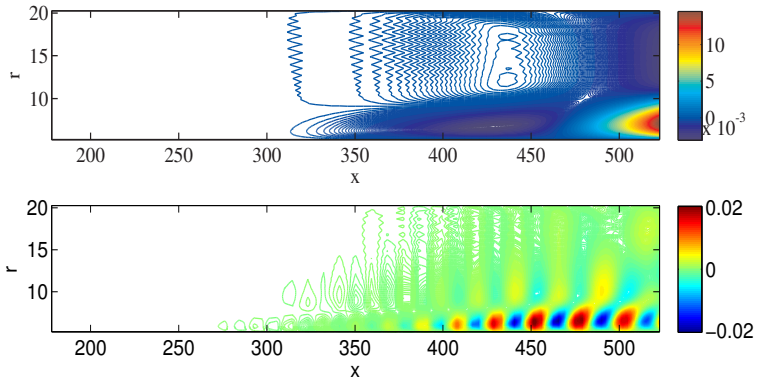

Figure 12: Contour plot of the real part of u for the two different eigenmodes associated with the frequencies (a) ω_r=0.003689 (b)ω_r=0.1234. The corresponding Reynolds number and azimuthal wave-number are Re=383 and N=0 respectively.

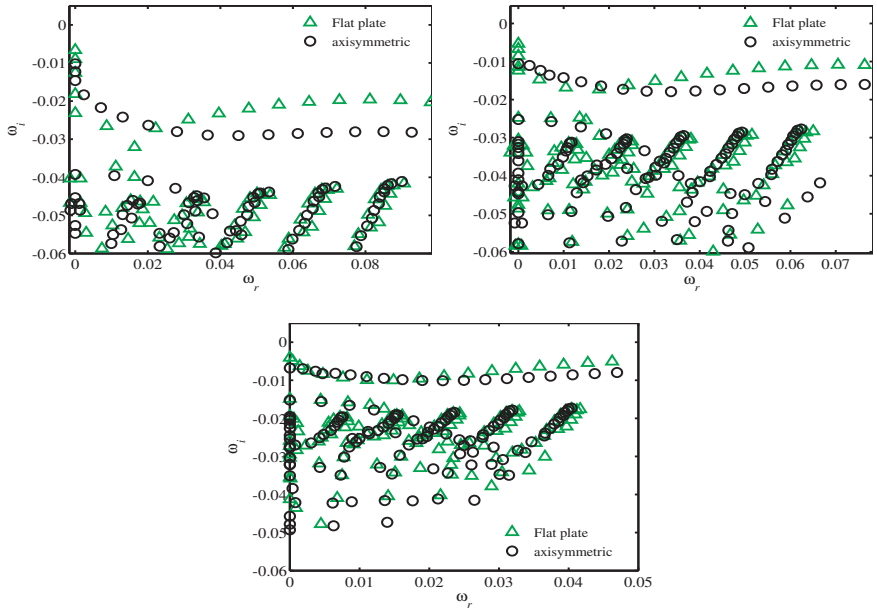

Figure 13: Comparison of eigenspectrum for axisymmetric (N=0) and 2D flat plate ($\beta = 0$) boundary layer for $L_{x=345}$ for three different Reynolds number (a) Re=383 (b) Re=557 and (c) Re=909.

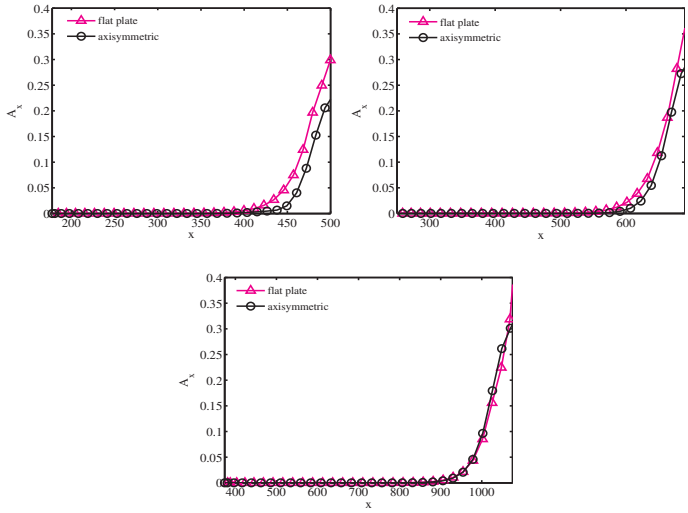

Figure 14: Comparison of spatial amplification rate of axisymmetric (N=0) and 2D flat plate ($\beta = 0$)boundary layer for three different Reynolds number (a) Re=383 (b) Re=557 and (c) Re=909.

shows the comparison of eigen spectrum for three different Reynolds numbers 383, 557 and 909 (based on the body radius of the cylinder these are 2000, 4000 and 10000) with L_x=345 for axisymmetric and flat plate boundary layer. The comparison is limited for the discrete part of the spectrum only. It has been observed that at small Reynolds number the damping rates of eigen modes are higher (ω_i is smaller) for axisymmetric boundary layer than that of flat plate boundary layer. The difference of damping rate in eigen modes for axisymmetric and flat plate boundary layer reduces with the increase in Reynolds number. The eigen modes of axisymmetric boundary layer approaches to eigen modes of flat plate boundary layer at higher Reynolds number. This is primarily due to the effect of transverse curvature only. The effect of transverse curvature is significant at low Reynolds number. The effect of transverse curvature reduces with the increase in Reynolds number. Thus, it proves that the global modes are more stable at low Reynolds number for axisymmetric boundary layer.

Figure 14 shows the comparison of spatial amplification rates (A_x)at three different Reynolds number for both the boundary layers. The least stable mode is selected to compute the spatial amplification rate. The comparison shows that at low Reynolds number, (A_x)is higher for flat plate boundary layer. The (A_x) for axisymmetric boundary layer also increases with the increase in Reynolds number and approaches to flat plate boundary layer at higher Reynolds number.

Three different families of eigenspectrum are shown in figure 15 for axisymmetric and flat plate boundary layer. The discrete part of the spectrum is only shown in the figures for the comparison. The difference between the spectrum depends on the domain length. The distance between two consecutive frequency reduces with the increase in domain length. To quantify this discretization of the eigen modes for Re=323, different domain lengths were considered with $L_{x1} = 345$,$L_{x2} = 475$ and $L_{x3} = 605$. Figure 16 shows the comparison of

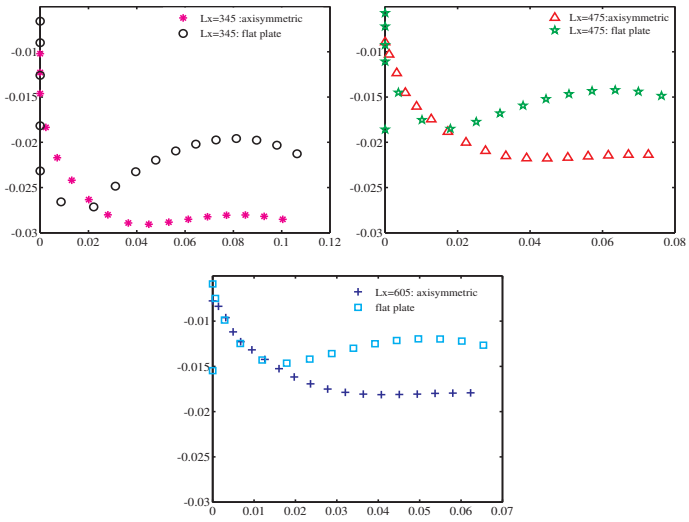

Figure 15: (a)Comparison of eigen spectrum for different stream-wise domain length for Re=383 for axisymmetric (N=0) and 2D flat plate boundary layer($\beta = 0$).

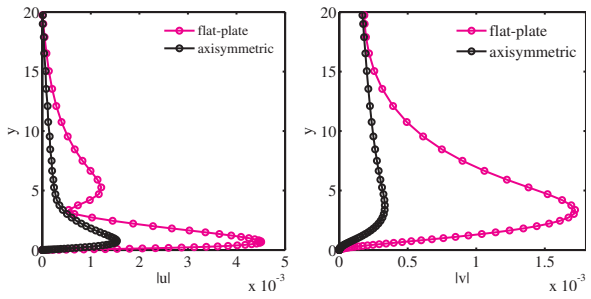

Figure 16: Comparison of modulus of eigen-function (a) u and (b) v at stream-wise location x=445 for Re=383 for axisymmetric (N=0) and 2D flat plate boundary layer($\beta = 0$).

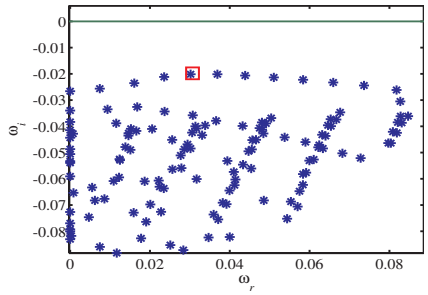

Figure 17: Eigenspectrum for azimuthal wavenumber N=1 and Re=383.

modulus of streamwise and normal disturbance velocity u and v respectively for Re=383 at x=445. The magnitude is modulus of disturbances is higher for flat plate plat boundary layer.

5.5 Helical mode (N=1)

The eigenspectrum for azimuthal wave number N=1 and $R_e = 383$ is shown in figure 17. Stationary eigen mode is also found corresponding to $\omega_r = 0$ in the non-axisymmetric case too. The corresponding growth rate ω_i is -0.02661. Figure 18 presents the global structure of disturbance amplitude of the oscillatory mode. The oscillatory mode with largest imaginary part is $\omega = 0.03654 - 0.01763i$. This global mode is also temporally stable because $\omega_i < 0$. The eigenmode corresponding to N=1 is non-axisymmetric and therefore, the disturbance velocity have azimuthal component (w) also. The spatial structure for streamwise(u), radial (v) and azimuthal(w) disturbance velocity amplitudes is shown in figure 18. The disturbance amplitudes grows in streamwise direction when moving towards the downstream. The magnitudes of the amplitudes also increases towards the downstream. The wave-like nature of the disturbance amplitudes is also found in figure 18.

5.6 Temporal growth rate

Figure 20 shows the temporal growth rate of the eigenmodes for different Reynolds number. The growth rate increases with the increase in Reynolds number for all the azimuthal wave numbers. As the largest imaginary part is negative for different Reynolds number the flow is temporally stable. The transverse curvature varies inversely with the Reynolds number. At low Reynolds number growth rate is small and with the increase in Reynolds number growth rate increases. Which proves that transverse curvature has significant damping effect on the global temporal mode also. A global modes with higher wave numbers, N=3,4 and 5 are more stable than that of axisymmetric and helical mode N=1 and 2. At low Reynolds number axisymmetric mode is having higher growth rate then that of N=1 and 2. As Reynolds number increases,the growth rate of helical mode N=1 and 2 increases then that of axisymmetric mode.

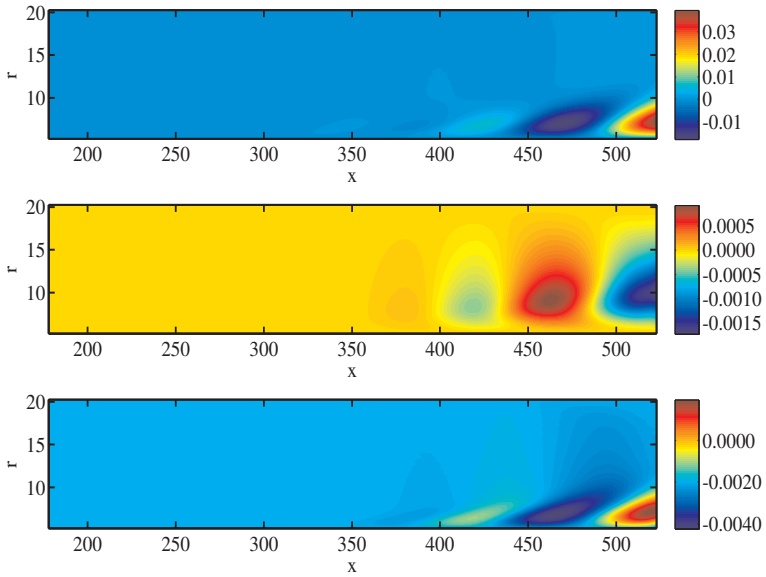

Figure 18: Contour plot of (a) streamwise(u) (b) radial (v) and (c) azimuthal (w), for disturbance velocity for oscillatory mode N=1 and Re=383. The associated eigenvlaues is $\omega = 0.03654 - 0.01763i$, as marked by square in figure 17.

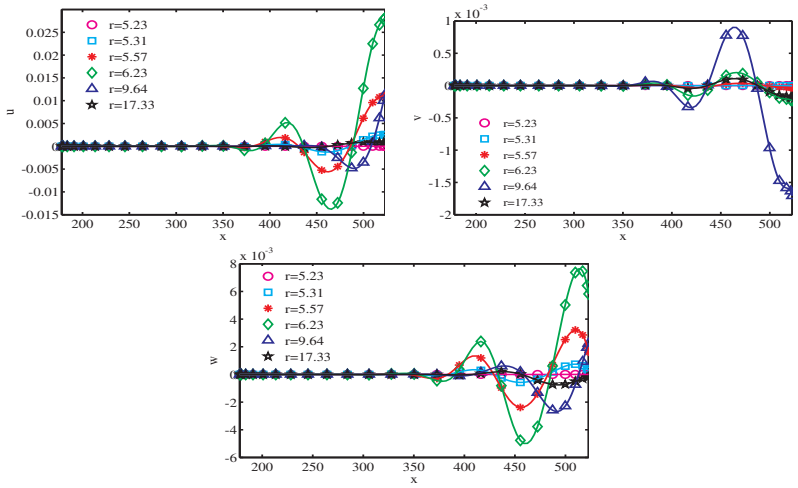

Figure 19: Variation of disturbance amplitudes in streamwise direction for (a) streamwise (u) (b) radial (v) and (c) azimuthal(w) disturbance amplitudes at different radial location $\omega = 0.03654 - 0.01763i$, as marked by square in figure 17.

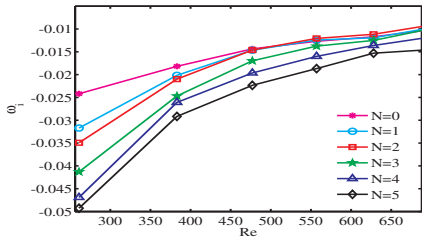

Figure 20: Variation in temporal growth rate (ω_i) with Reynolds number for different azimuthal wave numbers .

5.7 Spatial amplification rate

The global temporal modes exhibit spatial growth/decay in streamwise direction when moving towards the downstream. The disturbances in the streamwise direction at a particular radial location may decay or amplify. However the overall effect of all disturbances together at each streamwise location can be quantified by computing the spatial amplitude growth, A(x) [7].

$$A(x) = \sqrt{\int_1^{r_{max}} (u^*(x,r)u(x,r) + v^*(x,r)v(x,r) + w^*(x,r)w(x,r))dr} \quad (28)$$

where * denotes the complex conjugate. Figure 5.7 shows the spatial amplitude growth of the disturbance waves for different azimuthal wave numbers at various Reynolds number. Most unstable oscillatory ($\omega_r \neq 0$) temporal modes are considered to compute the spatial growth of the amplitudes. The amplitude growth increases in the streamwise direction as the flow is convectively unstable. At low Reynolds number the the growth of disturbances start at early stage.

6 Summary

The global temporal modes are computed using linear stability theory for axisymmetric boundary layer. The numerical eigenvalue problem is solved using ARPACK, which employs Arnoldi's iterative algorithm. The stability analysis conducted for various Reynolds number and azimuthal wave numbers. The largest imaginary part of the computed eigenvalues are negative for the range of Reynolds number and azimuthal wave numbers considered here. Thus the flow is temporally stable. The global modes in axisymmetric boundary layer, showed wavelike behaviour for the range of Reynolds numbers considered. The spatial properties of the global mode shows that the disturbances grow in size and magnitude within the flow domain in the streamwise direction when move towards the downstream, which hints that the flow is convectively unstable. At low Reynolds number axisymmetric mode (N=0) is least stable one, while at higher Reynolds number($Re > 577$) helical mode N=2 is observed least stable one. The global modes with higher wave numbers N=3, 4 and 5 are more stable. The comparison of global modes of axisymmetric and flat plate boundary layer shows that at low Reynolds number the effect of transverse curvature is significant, however with the increase in Reynolds number this effect reduces and global modes of the axisymmetric boundary layer become less stable. Thus, the

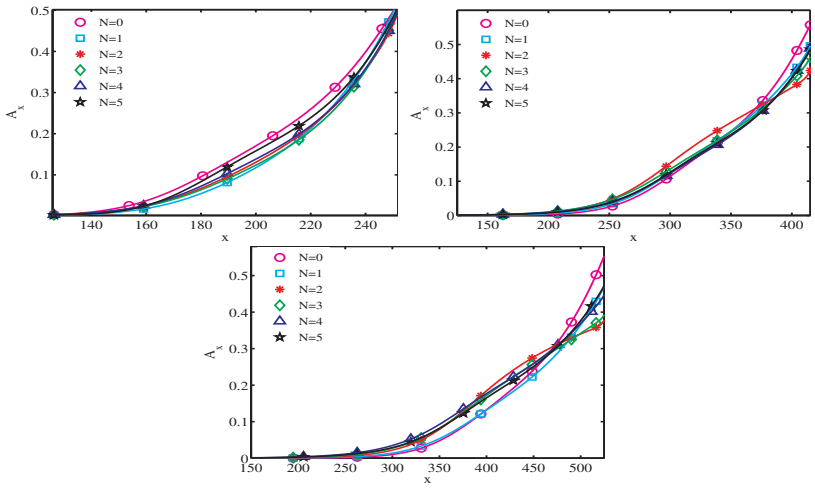

Figure 21: Spatial amplification rate A_x in streamwise direction x for (a) Re=261 (b) Re=477 and (c) Re=628 for different azimuthal wave numbers. The most unstable temporal mode is considered to compute the spatial amplitude growth A_x.

transverse curvature shows overall damping effect on the global modes. The amplitude functions corresponding to the stationary mode is found to be monotonically growing in the streamwise direction.

References

[1] Alizard, F., Robinet, J.C.: Speatially convective global modes in a boundary layer. Physics of Fluid **19**, 3229–3246 (2007)

[2] Bert, P.: Universal short wave instability of two dimensional eddies in inviscid fluid. Physical Review E. **57**, 2157–2159 (1986)

[3] Christodoulou, K.N., Scriven, L.E.S.: Finding leading modes of a viscous free surface flow: An asymmetric generalized eigenproblem. Journal of Scientific Computing **3**, 355–406 (1988)

[4] Costa, B., W., D., Simas, A.: Spatial resolution properties of mapped spectral chebyshev methods. Proc. SCPDE: Recent Progress in Scientific Computing pp. 179–188 (2007)

[5] Crighton, D.G., Gaster, M.: Stability of slowly diverging jet flow . J. Fluid. Mech. **77**, 397 (1976)

[6] Drazin, P., Reid, W.: Hydrodynamic stability. Cambridge Univerisity Press (2004)

[7] Ehrenstein, U., Gallaire, F.: On two-dimensioanl temporal modes in spatially evolving open flow :the flat-plate boundary layer. J. Fluid. Mech. **536**, 209–218 (2005)

[8] Fasel, H., Rist, U., U., K.: Numericla investigation of the three - dimensional development in boundary layer transition. AIAA J **28(1)**, 29–37 (1990)

[9] Glauert, M.B., Lighthill, M.J.: The axisymmetric boundary layer on a thin cylinder. Proc. Roy. Soc. London Ser. A **230**, 188–203 (2000)

[10] Jackson, C.: A finite-element study of the onset of vortex shedding in flow past variously shaped bodies. J. Fluid. Mech. **182**, 2345 (1987)

[11] Joseph, D.: Nonlinear stability of the boussinesq equations by the method of energy. Arch. Rat. Mech **22**, 163–184 (1966)

[12] Lin, R., Malik, M.R.: On the stability of attachment-line boundary layers. part 1. the incompressible swept hiemenz flow. J. Fluid. Mech. **311**, 239–255 (1996)

[13] Malik, M.: Numerical methods for hypersonic boundary layer stability. Journal of Computational Physics **86(2)**, 376–412 (1990)

[14] Malik M.R and Poll, D.: Effect of curvature on three dimensional boundary layer stability. AIAA Journal **23**, 1362–1369 (1985)

[15] Monokrousos, A., Akervik, E., H, H.: Global three dimensional optimal disturbances in the blasius boundary layer flow using time stepers. J. Fluid. Mech. **536**, 209–218 (2005)

[16] Rao, G.: Mechanics of transition in an axisymmetric laminar boundary layer on a circular cylinder. Journals of applied Mathematics and Physics **25**, 251–292 (1974)

[17] Roache, P.J.: A method for uniform reporting of grid refinment study. J. Fluid. Mech. **19**, 405413 (1994)

[18] Rodriguez, D., Theofilis, V.: On instability and structural sensitivity of incompressible laminar separation bubbles in a flat-plate boundary layer. AIAA 38th Fluid Dynamics Conference And Exhibit, Seattle, **4148** (2008)

[19] Swaminathan, G., Shahu, K., Sameen, A., Govindrajan, R.: Global instabilities in diverging channel flows. Theor. Comput. Fluid Dyn. **64**, 25–53 (2011)

[20] Tatsumi, T., Yoshimura, T.: Stability of the laminar flow in a rectangular duct. J. Fluid. Mech. **212**, 437–449 (1990)

[21] Tezuka, A., Suzuki, K.: Three-dimensional global linear stability analysis of flow around a spheroid. AIAA J. **44**, 1697–1708 (2006)

[22] Theofilis, V.: Advances in global linear instability analysis of nonparallel and three dimensional flows. Progress in Aerospace Sciences **39**, 3229–3246 (2003)

[23] Theofilis, V.: Global liniear instability. Annu. Rev. Fluid Mech. **43**, 319–352 (2011)

[24] Theofilis, V., Hein, S., Dallmann, U.: On the origins of unsteadiness and three dimensionality in a laminar separation bubble. Proc. Roy. Soc. London Ser. A **358**, 3229–3246 (2000)

[25] Tutty, O., Price, W.: Boundary layer flow on a long thin cylinder. Physics of Fluid **14**, 628–637 (2002)

[26] Vinod, N.: Stability and transition in boundary layers: Effect of transverse curvature and pressure gradient. Ph.D. thesis, Engineering Mechanics Unit, JNCASR (2006)

[27] Vinod, N., Govindarajan, R.: Secondary instabilities in incompressible axisymmetric boundary layers: Effect of transverse curvature. J.Fliud Eng. **134** (2012)

[28] Zebib, A.: Stability of viscous flow past a circular cylinder. Journal of engineering Mathematics **21**, 155–165 (1987)